

## RESULTS ON THE BEAM COMMISSIONING OF THE SUPERCONDUCTING RFQ OF THE NEW LNL INJECTOR

A. Pisent, G. Bisoffi, D. Carlucci, M. Cavenago, M. Comunian, A. Facco, E. Fagotti, A. Galatá, A. Palmieri, M. Poggi, A. M. Porcellato, P. A. Posocco, C. Roncolato, INFN/LNL, Legnaro, Italy  
S. Vitulli, CNAO Foundation, Milano, Italy

### Abstract

A new injector for the heavy ion superconducting linac ALPI has been built at LNL. This new accelerator, named PIAVE, is designed to accelerate ions with  $A/Q < 8.5$  up to 1.2 MeV/u. The main components are an ECRIS source operating on a high voltage platform, a three harmonic buncher, a superconducting RFQ cryomodule containing two bulk niobium structures and two QWR cryomodules housing 4 cavities each. In the last year the injector has been commissioned, with O, Ar, Ne and Xe beams, and put into operation. The beam performances, and the results of longitudinal and transverse emittance measurements will be shown and compared with simulations. Neon and argon beams have been delivered to the experiments (after acceleration with PIAVE and ALPI) for a total of about 200 hours. It should be noted that this is the first superconducting RFQ in operation; the design opportunities offered by this technology for a wider field of applications will be briefly discussed. The heart of these opportunity is given by the high intervane voltage in a cw RFQ (PIAVE can operate cw with an intervane voltage higher than 250kV).

### PIAVE COMMISSIONING

The commissioning of the Positive Ion Accelerator for low-Velocity Ions (PIAVE) [1] with various beam species was completed in early spring 2006. Starting from October 2006, the first official nuclear physics experiments with PIAVE Injector will be scheduled by the international Programme Advisory Committee.

The new injector is based on superconducting RFQs (SRFQs) [2] [3] [4], which are used here for the first time. The SRFQs are followed by eight SC Quarter Wave Resonators (QWRs). The beam, received from an ECR source on a 350kV platform, is bunched between the ECR and the SRFQs and re-bunched between PIAVE and the SC booster ALPI by normal conducting cavities [5]. In Fig. 1 is shown a photo of the complex, and in Fig. 2 the lay-out of the injector.

The injector setup started in November 2004 with a  $^{16}\text{O}^{3+}$  pilot beam. In December 2005, after a long shutdown of the ALPI booster cryogenic plant, a very first  $^{22}\text{Ne}$  test beam was accelerated by PIAVE and ALPI to the experimental apparatus PRISMA-Clara (final energy  $\sim 6\text{MeV/A}$ ), where it provided stable beam-on-target conditions for around 50 hours, before scheduled conclusion.

In the period January-April 2006, the LNL tandem-ALPI operation programme allotted around 5 days/month

for PIAVE+ALPI beam tests. In this period, tests with  $^{22}\text{Ne}$ ,  $^{132}\text{Xe}$ ,  $^{40}\text{Ar}$  and  $^{84}\text{Kr}$  beams were conducted. Final energy on target ranged between 5 and 8.25 MeV/A and currents between 5 and 15 pA. The typical time required driving the beam through injector and booster to the experimental station was  $\sim 36$  hours.

The period May-July 2006 was dedicated to maintenance on the SRFQ cryostat and the TCF50 cryogenic system. Meanwhile the tandem-ALPI complex provided ion beams to user stations, allowing recovering most of the shifts lost during the long shutdown of 2005.



Figure 1: Photo of the completed injector PIAVE

### RFQ DESIGN CHARACTERISTICS

The heart of the new injector [6] is the superconducting RFQ section. The main design parameters are summarized in Tab. 1. The beam is pre-accelerated in a 312kV platform and bunched with an external three harmonic buncher (40, 80, 120MHz) with the possibility of implementing a 5MHz bunching system for TOF measurements later.

The SRFQ, without a complete bunching section, has been optimized to achieve a high accelerating gradient, since power losses are negligible and the cost of the structure and associated cryostat is rather high. This result has been obtained by splitting the RFQ in two independent cavities. In SRFQ2, thanks to the increased  $\beta$ , both the intervane voltage  $V$  and the aperture  $R_0$  are almost doubled. In this second structure (with  $V=280\text{kV}$ ) the accelerating field exceeds 2.8 MV/m, which is to our knowledge the world record for an RFQ, and the normalized transverse acceptance exceeds 2.5 mmmrad.

The two SRFQ resonators are of ladder kind, with four stems per electrode in SRFQ1 and two in SRFQ2; the transverse dimensions are therefore almost the same. The field configuration of the operating mode in these

resonators is pretty insensitive to geometric errors, since in the worst case the resonator length is  $0.37\lambda$  and the dipoles are 10MHz higher in frequency. It is instead very critical the tuning of the operating mode frequency (starting from an achieved mechanical accuracy better than  $50\mu\text{m}$  in the welded assembly) and the stiffening of the system against vibrations.

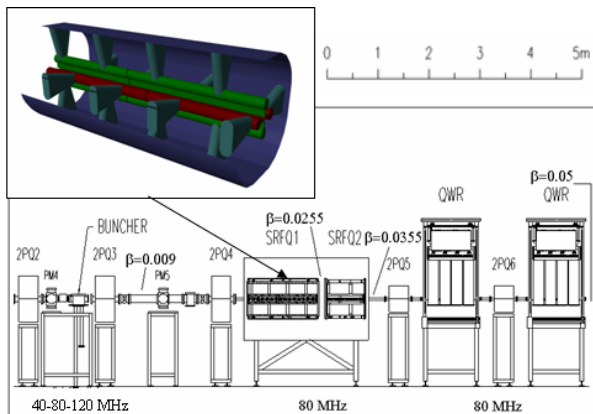


Figure 2: Lay-out of PIAVE (accelerating structures).

The physical distance between the two SRFQs (200mm) determines a transverse beam mismatch in SRFQ2 (where the acceptance is large). This mismatch has been minimized interrupting SRFQ1 in a point where the Twiss parameter are  $\alpha_x = \alpha_y = 0$ . Longitudinally instead the phase advance is matched with the correct choice of the synchronous phase of SRFQ2. Moreover in the transition region we profit of an additional acceleration specific of these alternating stem structures [7].

Table 1: SRFQ main parameters.

Mass to charge ratio	8.5		
Beam current	<5	$\mu\text{A}$	
RMS Emittance	0.1	mmrad	norm.
Radio Frequency	80	MHz	
Input Energy	37.1	keV/A	$\beta = .0089$
Max. Surface field	25	MV/m	
Max. stored energy	$\leq 4$	J/RFQ	
Band width	>20	Hz	
	<b>SRFQ1</b>	<b>SRFQ2</b>	
Vanes length	137.8	74.61	cm
Output energy	341.7	586	keV/A
Voltage	148	280	kV
Tank diam. (approx)	65	65	cm
Number of cells	42.6	12.4	
Average aperture $R_0$	0.8	1.53	cm
Modulation factor m	1.2-3	3	
Synchronous Phase	-40 $\div$ -18	-12	deg

Following the SRFQ (at  $\beta=0.355$ ) the beam enters directly the QWR section. The longitudinal matching is here achieved using the first cavity as a buncher, and with alternating phase focusing. The synchronous phase sequence is (-90,+20,+20,+20,-20, -20, +20, +20). This

approach allows a compact system, but is sensitive to alignment errors that can easily result in important longitudinal emittance increase.

Finally the beam is transported into ALPI superconducting linac through a  $90^\circ$  achromatic bending and longitudinally matched with two nc QWR bunchers.

## BEAM COMMISSIONING RESULTS

Beam tests were carried out in three steps, with different positions of a temporary emittance measuring unit (EMU): at the SRFQ input [8], after the SRFQ [9] and after the QWRs. The beam has therefore been transported into ALPI up to the experiments.

The EMU contains two slit and harp BPM (44 channels) systems moving along x and y direction, a FC and a Si detector. In addition PIAVE is equipped with 8 permanent measurement positions, with harp BPM and FC. Finally, in the third commissioning phase the beam could be transported after the first  $45^\circ$  dipole of the bend to ALPI (with NMR field measurement) and analysed in energy.

The two PIAVE SRFQs have been tuned with  $^{16}\text{O}^{3+}$  beam and the external buncher off, recording beam transmission (on FC) and energy spectrum (on Si detector) for different phases of SRFQ2 (Fig. 3); a current of  $\sim 1\text{-}3\mu\text{A}$  was typically available from the source.

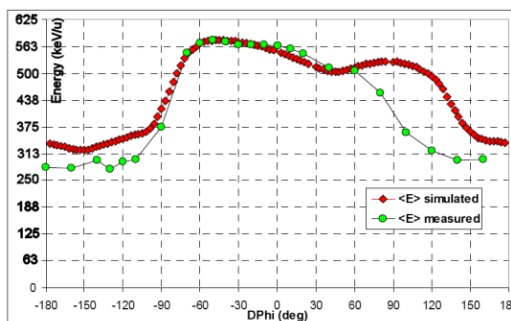


Figure 3: Simulated and measured ( $^{16}\text{O}^{3+}$ ) average energy at RFQ exit as function of SRFQ2 phase (buncher off).

It should be noted that the quadrupole doublet 2PQ5, located after the SRFQs and before the EMU, determines a certain energy selection due to chromaticity. This effect is taken into account in the PAMTEQM-PARMILA simulations superimposed to the measurements in Fig. 3.

Simulations and measures match very well in the phase range in which the SRFQ1 beam falls within the SRFQ2 separatrix, allowing a precise determination of the nominal SRFQ2 phase. After this phase regulation, the buncher has been switched on to the nominal voltages and adjusted in phase so to reach the maximum transmission.

The values of transmission reached in January 2005 were in the 40-45% region, in disagreement with simulations that predicted a 68%. It was hence decided to realign the LEBT respect to the RFQ, checking both with optical devices and with best beam transmission (Fig. 4).

For various positions of the last LEBT doublet, each point corresponds to the best transmission optimized

respect to the values of many parameters, like steerer fields and buncher cavity phases. At the end of this process, the beam transmission predicted by simulations has been achieved.

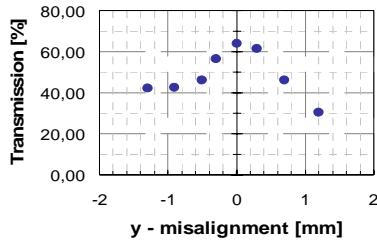


Figure 4: Beam transmission as a function of the vertical position of the last magnetic doublet.

*Emittance measurements*

After phase tuning, the SRFQs have been completely characterized through a set of transverse and longitudinal emittance measurements for different beams. In Tab. 2 the results for  $^{40}\text{Ar}^{9+}$  and  $^{16}\text{O}^{3+}$  after the RFQ are presented. These values are perfectly consistent with LEBT beam measurements and RFQ simulations.

Table 2: Transverse Normalized Emittance at SRFQs exit.

Ion	$E_{\text{RMS},x}$ [mm-mrad]	$E_{\text{RMS},y}$ [mm-mrad]
$^{40}\text{Ar}^{9+}$	0.10	0.10
$^{16}\text{O}^{3+}$	0.11	0.12

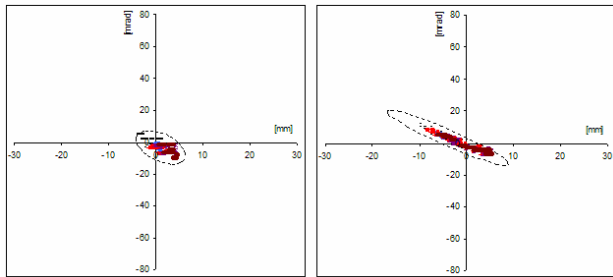


Figure 5:  $^{16}\text{O}^{3+}$  beam horizontal and vertical emittance after the RFQ.

Longitudinal emittance has also been measured in the same position, using a silicon detector intercepting the particles scattered at  $25^\circ$  angle by a thin golden foil. The data acquisition system allows to determine the time-energy correlations with the possibility (in principle) to get a direct plot of the longitudinal emittance. In practice, while the bunch length measured seems correct, we have not yet been able to get an acceptable energy resolution.

The comparison of the energy spread of an Ar beam after the RFQ as foreseen by simulations, as measured with silicon detector and as measured with magnetic dispersion after the dipole PD3 indicates that the silicon detector overestimates of an order of magnitude the energy spread. The spread from simulation is  $\Delta W/W=0.3\%$ , while Si measurement gives  $\Delta W/W=9.0\%$  and magnetic dispersion  $\Delta W/W=0.6\%$ . As a consequence the rms emittances measured with time-energy correlation of Si detector signals are overestimated. We have

therefore decided to measure the longitudinal emittance indirectly, following the three gradients method, changing the field of the third QWR cavity, used as a buncher with  $\phi_s=-90^\circ$  (see Fig. 6).

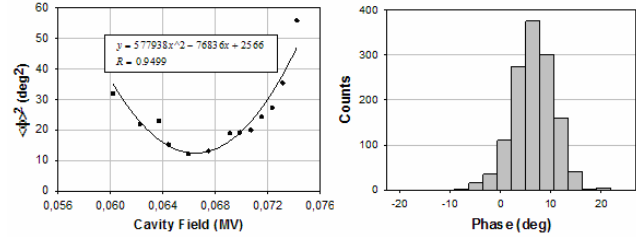


Figure 6: Bunch length as function of the field of the third QWR used as buncher and bunch shape at minimum.

The computed emittances are reported in Tab. 3. The three gradients method instead gives an emittance value that is within a factor 2.5 in agreement with what expected from simulations for a perfectly aligned machine. This result is encouraging and shows that the SRFQ can give a longitudinal emittance perfectly comparable with the performances of the other heavy ion injectors. Deeper investigations will be done in the next MD shifts.

Table 3: Longitudinal emittance measured using  $^{40}\text{Ar}^{9+}$  beam (the statistical error is indicated).

	$\epsilon_{\text{RMS},l}$ [deg-keV/u]	$E_{\text{RMS},l}$ [ns-keV/u]
Direct meas.	$39 \pm 1.6$	$1.358 \pm 0.006$
3 Grad. meth.	$5.5 \pm 0.3$	$0.19 \pm 0.01$
Sim. results	2.16	0.075

*Operation of SRFQ and QWR cavities*

SC RFQs were conditioned up to the design surface field required by the reference  $^{238}\text{U}^{28+}$  beam, i.e. 25.5MV/m, corresponding to a dissipated power of  $\sim 10$  W at 4.5K. Residual field emission is present in SRFQ2 at this field level. However,  $E_s=22\text{MV/m}$  (i.e. 86% of the nominal value) was reliably used, for time spans of around 5 days, for the above mentioned  $^{22}\text{Ne}^{3+}$  and  $^{132}\text{Xe}^{18+}$  beam tests.

QWRs [10] reached off-line accelerating field of  $\sim 7\text{MV/m}$  ( $E_s/E_a \sim 5$ ), while their nominal accelerating field in PIAVE is 5MV/m. Beam dynamics considerations suggest scaling the accelerating field of QWR with the q/A ratio as for the RFQ. Therefore, we used in operation a field as high as 4.3MV/m on the 8 QWR of PIAVE, also with several days of stable conditions.

Phase and amplitude locking asks for an enlargement of the resonant bandwidth on all cavities. This was achieved: on QWRs, by over-coupling the SC cavity in a self-excited loop (SEL) mode (100÷300W amplifiers were used); on SRFQs, using VCX fast tuners [11].

For what concerns PIAVE cryogenic plant (based on a LINDE TCF 50 refrigerator able to supply a power of 410W at 4.2K and 1000W at 80K) a fine tuning work performed in collaboration with Linde Kr. AG allowed achieving pressure variations smaller than 2mb/min.

Such a drift is slow enough, to allow compensating the related frequency drifts of all SC resonators by means of their mechanical tuners.

As a conclusion of the several beam tests of the latest months, it is noted that, for all resonators (both SRFQ and QWR), unlocking is an extremely rare event (less than once a day), while one or two times per hour, on average, phase and amplitude errors typically exceed their maximum values (0.4deg in phase and 0.25% in amplitude), for a few seconds at most and recover automatically, without any operator action.

### ACCELERATION IN PIAVE-ALPI

After the long shutdown of the ALPI cryogenic plant, in Autumn 2005 PIAVE beams have been accelerated in ALPI. The available acceleration, due to various limitations, corresponds to an average accelerating field of ~3.MV/m (12 bulk Nb cavities operating at 80 MHz with  $\beta=0.056$ , 54 Nb sputtered on Cu operating at 160MHz, 44 with  $\beta=.11$  and 8 with  $\beta=.14$ ); for each cavity the effective length is 0.18m. The beam energy and current delivered to users are quoted in Tab. 4 and plotted in Fig. 7. In the same plot is also shown the maximum energy reachable (keeping PIAVE with constant phases, final energy 1.2MeV/A).

Table 4: Beams delivered to users.

Beam	A/Q	Into exp.		
		pnA	MeV/A	hours
<sup>40</sup> Ar <sup>9+</sup>	4.4	7.8	6.25	30
<sup>40</sup> Ar <sup>9+</sup>	4.4	0.44	8.25	76
<sup>22</sup> Ne <sup>4+</sup>	5.5	1	6	50
<sup>22</sup> Ne <sup>3+</sup> ( <sup>132</sup> Xe <sup>18+</sup> )	7.3	20	5	Not req.

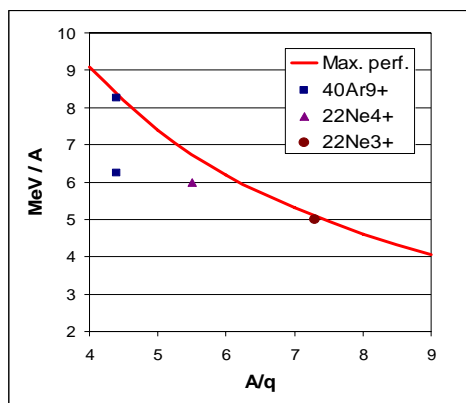


Figure 7: PIAVE beam; the red curve corresponds to the ALPI acceleration presently available (see text).

ALPI has instead been operated at fixed accelerating field. Therefore for each beam (with different A/q ratio) a specific beam dynamics had to be found with multiparticle simulations (PARMELA); in most cases indeed the beam dynamics was not predictable with matrix transport codes, due mainly to the important role of Bessel functions in the accelerating gaps. To help the transverse focusing it is necessary a specific choice of the synchronous phase of the 8 cavities of the period between

-20° and +20°. In all cases we obtained a good transverse matched envelope whereas the longitudinal solution was not periodic and satisfied the only requirement of a tight RMS phase envelope (<10°). The quality of the overall result was monitored in simulations by the emittance growth, that we kept less than 10% per period; such condition is critical at low energy. In the second part, when the beam energy reaches the 3.5MeV/A, the envelope can be matched to a standard periodic solution as shown in Fig. 8.

The transmission reached in operation applying these solutions was fair, even if some alignment and hardware problems came into evidence and will be faced in the next shut down. Up to now the typical beam transmission from ECR source to experiments is 15%.

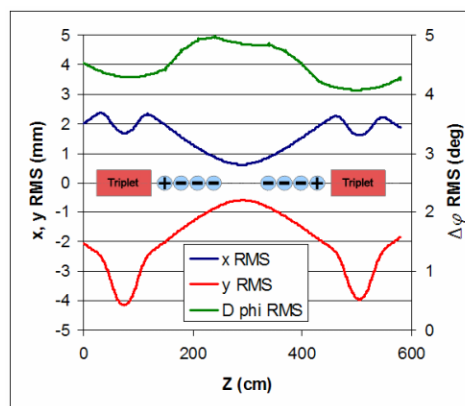


Figure 8: Typical beam envelopes for one of the ALPI accelerator periods, composed by one quad triplet and 2 cryomodules, 8 QWR (tuned at  $\phi_s +$  or  $-20^\circ$  as indicated).

### FUTURE PERSPECTIVES

The successful operation of PIAVE SRFQs opens new possibilities for the applications of these accelerators characterized by high voltage, high accelerating field and large transverse acceptance [12]. We concentrate here on structures operating at ~80 MHz that can immediately use most of the technological development available.

The first application is related to the post-acceleration of Radioactive Ion Beam (RIB) produced in a ISOL (Isotope Separation On Line) facility, as proposed for the LNL project SPES. RIBs generated ionizing the gas released by a hot target, are weak, costly and continuous (the memory of the primary accelerator time structure is lost in the gas diffusion).

In this case a SRFQ is a very competitive choice for the first element of the superconducting linac. Respect to PIAVE lay-out one has to consider that the RIB production ion source will lay at a voltage of 20-60kV, so that a bunching RFQ before SRFQ1 is needed (up to 37keV/u). Such bunching RFQ, studied by LNL group within EURISOL design study, can be built both nc or sc, and has the advantage of collecting virtually 100% of the precious secondary beam into the post accelerator acceptance.

As a second possible application we considered an SRFQ as first element of a 3-5 mA deuteron cw superconducting linac. Accelerators of this kind (final energy ~40MeV), for the production of neutrons and RIBs, are under construction in at least two laboratories. They require a cw RFQ that, being nowadays normal conducting, has a power consumption comparable with the rest of the linac for a rather modest beam power. An SRFQ in this case, operating in a system where a cryogenic system is anyway present, beside reducing the power consumption, allows to decrease substantially the beam losses and to increase the linac input energy (allowing a more robust beam dynamics).

Indeed for a deuteron RFQ beam losses should be kept well below 1% for radiation protection reasons. At the same time in a SRFQ the beam losses are even more severely limited by the heat deposition allowed in the cryostat (~20W). But fortunately the large transverse acceptance of SRFQs allows to design a beam dynamics with very small losses. In Tab. 5 a possible set of parameters is shown. The beam losses are  $<10^{-3}$ ; in Fig. 9 the PARMTEQM simulation is shown, where the very large space between beam envelope and structure aperture can be appreciated.

Table 5: Deuteron SRFQ main parameters.

Deuterons current	5	mA
Operating frequency	88	MHz
Input/output energy	0.022/1.3	MeV/A
Input/output emit. (norm. rms)	0.2	mmmrad
Output emit. (rms)	0.08	MeV deg/A
Beam losses	$<10^{-3}$	
RF power (beam loading *1.2)	15.3	kW
beam losses allowed	20	W
Intervane voltage V	217	kV
Average/minimum aperture	1.25/0.63	cm
Structure length	4	m
Maximum surface field	25	MV/m

Regarding the resonator we have considered here a structure almost identical to PIAVE RFQ, with some improvements necessary to realize a longer structure in a single resonator. The geometry is shown in Fig. 10 with cell length  $L_c=40.5\text{cm}$ , lower stem radius  $R1=3.5\text{cm}$ , upper stem radius  $R2=8.0\text{cm}$  and tank radius  $R=32.0\text{cm}$ . With respect to PIAVE RFQ the stems are positioned in the “in-line” configuration, rather than opposite. In this way, the tank can be divided in segments by means of joints to be put at half the cell length, where the longitudinal currents vanish due to symmetry reason. In Fig. 10 the HFSS simulations of the resonator show that the low B field region for the joint is not too small. This RFQ could for instance be realized in three tanks with the same length of PIAVE SRFQ1.

The application of SRFQ to an even higher beam current, such as for IFMIF class RFQs (~130mA), is at the moment very difficult to conceive, since it is even

difficult to have RFQ simulations reliable on the  $10^{-5}$  scale. But future is full of surprises!

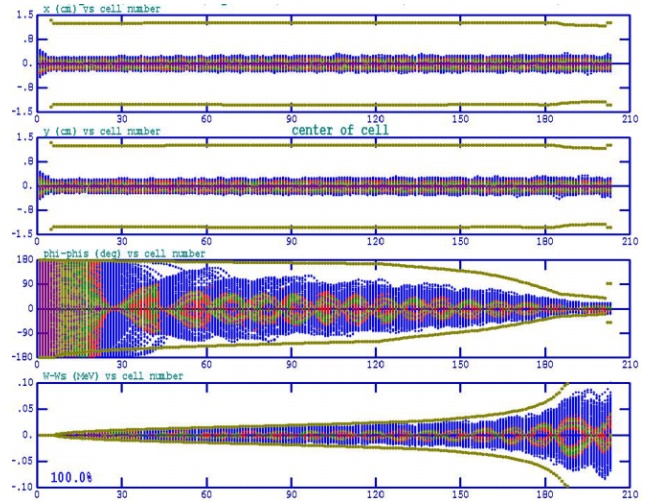


Fig. 9: PARMTEQM simulation of the d SRFQ: x, y,  $\delta\phi$  and  $\delta w$  coordinate vs. cell number.

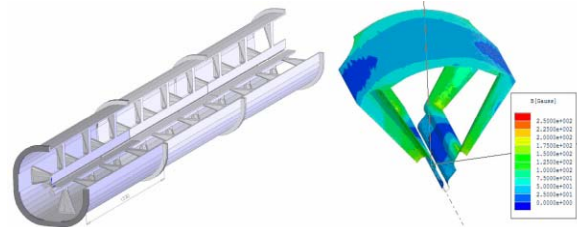


Figure 10: Sketch of the d SRFQ and B field dist. (HFSS).

## REFERENCES

- [1] A. Lombardi et al., Proc. of Linac2000, Monterey, USA, 356.
- [2] I. Ben-Zvi, A. Lombardi and P. Paul, Particle Accelerators, 1991, Vol. 35, pp. 177-192.
- [3] G. Bisoffi et al., Proc. of the SRF 2001 Workshop, 123.
- [4] G. Bisoffi et al., Proc. of Linac04, Lübeck, Germany, 623.
- [5] A. Facco et al., Proc. of EPAC 2000, Vienna, Austria, 2037.
- [6] A. Pisent, Proc. of the 8<sup>th</sup> International Conference on Heavy Ion Accelerator Technology (1998), AIP Conf. Proc. 473, 214.
- [7] A. Pisent and M. Comunian, Proceedings of PAC97, Vancouver, Canada, 1132.
- [8] A. Pisent et al., Proc. of EPAC 2000, Vienna, Austria, 1702.
- [9] A. Pisent et al., Proceedings of PAC05, Knoxville (Tennessee, USA), 2696.
- [10] A. Facco et al., Proc. of EPAC 2002, Lucerne, Switzerland, 2086.
- [11] V. Andreev et al., Proc. of EPAC 2000, Vienna, Austria, 2013.
- [12] A. Pisent et al., Proc. of Linac2000, Monterey, USA, 959.